Journal of
Nanoscience and Nanotechnology
Vol. 8, 1126–1137, 2008

REVIEW

Recent Progress on the Spectroscopy of Rare Earth Ions in Core–Shells, Nanowires, Nanotubes, and Other Novel Nanostructures

Xueyuan Chen[1,2,*], Liqin Liu[1], and Guokui Liu[2]

[1] State Key Laboratory of Structural Chemistry and Key Laboratory of Optoelectronic Materials Chemistry and Physics, Fujian Institute of Research on the Structure of Matter, Chinese Academy of Sciences, Fuzhou, Fujian 350002, China
[2] Chemistry Division, Argonne National Laboratory, Argonne, Illinois 60439, USA

Research and development of nanoscale luminescent and laser materials are part of the rapidly advancing nanoscience and nanotechnology. Because of unique spectroscopic properties and luminescent dynamics of *f*-electron states, doping luminescent rare earth ions into nano-hosts has been demonstrated as an optimistic approach to developing highly efficient and stable nanophosphors for various applications. In this article, we review the most recent progress in spectroscopic measurements of rare earth ion-activated low-dimensional nanostructures including nanolayers, core–shells, nanowires, nanotubes, and nanodisks. Among a large volume of work reported in the literature on many members of the rare earth series including Ce^{3+}, Pr^{3+}, Nd^{3+}, Eu^{3+}, and Er^{3+}, we focus on recent findings in the spectroscopic and luminescence properties of Eu^{3+} doped nanolayers, core–shells, and nanotubes, because Eu^{3+} ions have been extensively studied and widely used as an ideal probe for fundamental understanding of nano-phenomena. Specifically, the dependence of the optical properties of rare earth ions on nanostructures is discussed in detail.

Keywords: Rare Earth, Optical Spectroscopy, Luminescence, Excited State Dynamics, Nanocrystals.

CONTENTS

1. INTRODUCTION

Recently, rare earth (RE) ions doped in various low-dimensional nanostructures including core–shells, one-dimensional (1D) nanowires and nanotubes, two-dimensional (2D) nanofilms, hollow nanospheres, and 2D nanosheets and nanodisks have attracted extensive research interest because of their potential application in many fields.[1–4] This type of nanomaterials could play a vital role in the field of high performance luminescent devices, novel optical devices, catalysts, and biological labels and may also be used as a probe for determining how the size and morphology of nanoparticles affect their electronic structures and excited state dynamics, including radiative and nonradiative lifetimes, energy transfer, and thermalization phenomena.[4] It is expected that their unique structures could result in unusual mechanical, electronic, optical and magnetic properties.

The impact of the nanometer size effect on the spectroscopy of RE ions in insulating nanocrystals has been recently reviewed.[1,2,4] Novel optical properties, such as luminescence from new emerging sites,[5–10] prolonged luminescence lifetime,[11,12] anomalous thermalization,[13,14] upconversion luminescence,[15–28] long range interaction with two-level systems (TLS),[29–31] and improved quantum efficiency,[32,33] have been observed in RE-doped 0D and 1D nanocrystals. So far most reported studies are conducted for Eu^{3+} and Er^{3+} ions. Much attention is focused on the optical properties of Eu^{3+} ions since Eu^{3+} ion is a very good spectroscopic probe. In this paper, we report

*Author to whom correspondence should be addressed.

1533-4880/2008/8/1126/012 doi:10.1166/jnn.2008.306

recent advances in spectroscopic characteristics of RE ions in various nanostructures and different types of materials.

2. CORE–SHELLS OR NANOLAYERS

The core–shell technique has been extensively applied to the synthesis of both semiconducting and insulating nanostructures for a variety of purposes. By modifying their nanostructures, one can improve the quantum efficiency of RE optical centers, and design biolabels via biofunctionalization. Similarly, using the technique of chemical nanocoating, it is possible to alter the intrinsic properties of materials that cannot be achieved by conventional methods. Generally the core–shell nanostructures are divided into two categories: (I) RE doped in the core[28, 34–38] and (II) RE doped in the shell.[39–53] The former is synthesized in order to improve the quantum efficiency of RE ions or design biolabels,[54, 55] while the latter is synthesized for the study of surface modification on the RE luminescence or the synthesis of RE doped hollow nanospheres.

2.1. Eu^{3+}:Y_2O_3 Nanolayers Coated on Dielectric Nanoparticles

Recently, we have compared the structural and optical properties of Eu^{3+}:Y_2O_3 films coated on a variety of dielectric nanoparticles (Category II) using transmission electron microscope (TEM), X-ray diffraction (XRD) and site-selective, laser spectroscopy.[43, 44, 46] Eu^{3+} ions are employed as a probe for the study of crystallization and multi-site structure as well as the luminescent centers in nanolayers. It is observed that the luminescent

Xueyuan Chen received his B.Sc. degree in Material Chemistry from University of Science and Technology of China, Hefei, China, in 1993 and his Ph.D. in Physical Chemistry from Fujian Institute of Research on the Structure of Matter (FJIRSM), Chinese Academy of Sciences, Fuzhou, China, in 1998. His Ph.D. work focused on the optical spectroscopy and crystal-field analysis of rare earth doped laser crystals. He received an outstanding President award from the Chinese Academy of Sciences in 1997. After receiving his doctorate he joined FJIRSM as a research scientist and conducted research in the fields of solid-state laser and luminescent materials from 1998 to 2001. From 2001 to 2005, he was a postdoctoral research associate at the Chemistry Division of Argonne National Laboratory, U.S. Department of Energy, where he studied the photophysics and photochemistry of heavy elements with an emphasis on the laser spectroscopy of lanthanide-doped nanomaterials. In 2005, he joined the faculty at FJIRSM, where he is currently research professor of Material Chemistry and Physics. Chen's recent research interest is focused on the synthesis, characterization, and optical spectroscopy of rare earth ions embedded in the low-dimensional nanomaterials including insulator, semiconductor and core–shell nanocrystals. Dr. Chen has authored more than 50 journal publications, two book chapters, co-author of a book on the spectroscopy of laser and luminescent materials, and four Chinese patents related to solid-state lasers and nanotechnology.

Liqin Liu received her B.Sc. degree in Chemistry from Fujian Normal University, Fuzhou, China, in 2004. She is currently pursuing her Ph.D. in Material Chemistry and Physics at Fujian Institute of Research on the Structure of Matter, Chinese Academy of Sciences. Her research centers on synthesis, characterization, and optical spectroscopy of rare earth ions doped insulator nanocrystals. She has authored several SCI journal papers on rare earth spectroscopy.

Dr. Guokui Liu is a physicist and Principal Investigator of Chemistry Division of Argonne National Laboratory. His research interest is focused on experimental and theoretical studies of the electronic properties of lanthanides and actinides in condensed phases with an emphasis in modeling ion-ligand and electron–phonon interactions. He has managed research programs supported by the DOE Office of Science and aimed at achieving a predictive understanding of f-elements electronic energy level structure, excited-state dynamics, energy and charge transfer, and collective phenomena in both bulk and nanocrystals. Dr. Liu has also been leading applied research to address the long-term effects of nuclear radiation and improve the luminescence efficiency of nanophosphors. He has authored or co-authored more than 100 journal papers and edited three books in the field of chemical physics and materials science.

nanolayers exhibit distinct thermodynamics and luminescence properties.

Nanolayers of Eu^{3+}-doped Y_2O_3, were deposited on Al_2O_3, SiO_2, and ZnO nanoparticles by chemical deposition. The microscopic structures of Eu^{3+}:Y_2O_3 coating films on Al_2O_3 nanoparticles, prepared by three different methods (ammonia-aided hydrolysis, urea-aided hydrolysis, and direct evaporation), have been compared. It is shown that Eu^{3+}:Y_2O_3 nanolayers coated on alumina nanoparticles synthesized by the ammonia-aided hydrolysis method, with main cubic Y_2O_3 structure, are more homogeneous than those products synthesized by direct evaporation or urea-aided hydrolysis methods.[44]

2.1.1. Al_2O_3 Nanoparticles as Cores

Eu^{3+}:Y_2O_3 (2.5 at%) nanolayers coated on Al_2O_3 nanoparticles were synthesized by ammonia-aided hydrolysis followed by annealing the as-prepared sample at 750 °C for 12 h. Figure 1(a) shows the TEM image of the coated Al_2O_3 nanoparticles with an average particle size of approximately 60–70 nm. The high-resolution TEM (HRTEM) image of a selected nanoparticle before annealing (Fig. 1(b)) shows that the coating layer is approximately 6–8 nm. By isomorphic substitution, Eu^{3+} ions in cubic Y_2O_3 occupy two types of sites, a low symmetry C_2 site and a centrosymmetric S_6 site. There are about three times as many ions at the C_2 site as at the S_6 site. Besides, structural distortion in nanocrystals is expected because of the large surface-to-volume ratio and surface defects. The site-selective emission spectra of the sample are compared in Figure 2. The excitation and absorption spectra of Eu^{3+} in bulk Y_2O_3 crystal indicate no absorption at 355 nm. However, when the coated samples were pumped by a 355 nm laser, typical sharp transition peaks from $^5D_0$ of the Eu^{3+} ions at the C_2 site superimpose on the spectra arising from other sites such as surface sites, as shown in Figure 2(a). This is quite possibly due to energy transfer from the other sites to C_2 site. Energy levels (below 20,000 cm^{-1}) of Eu^{3+} ions at C_2 site in Y_2O_3

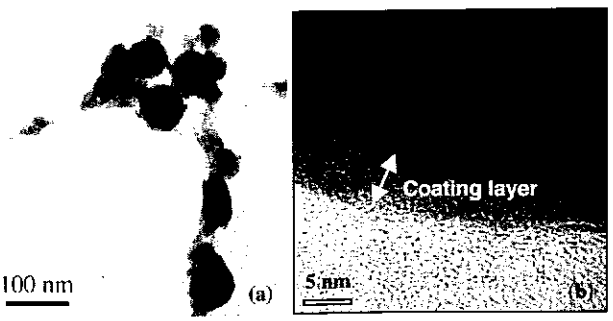

Fig. 1. (a) Bright-field TEM images of the as-prepared Eu^{3+}:Y_2O_3/Al_2O_3 nanolayers; (b) a high-resolution TEM image of the coating layer in a selected nanoparticle. Reprinted with permission from [43], X. Y. Chen et al., *Nanotechnology* 14, 670 (**2003**). © 2003, Institute of Physics and IOP Publishing Ltd.

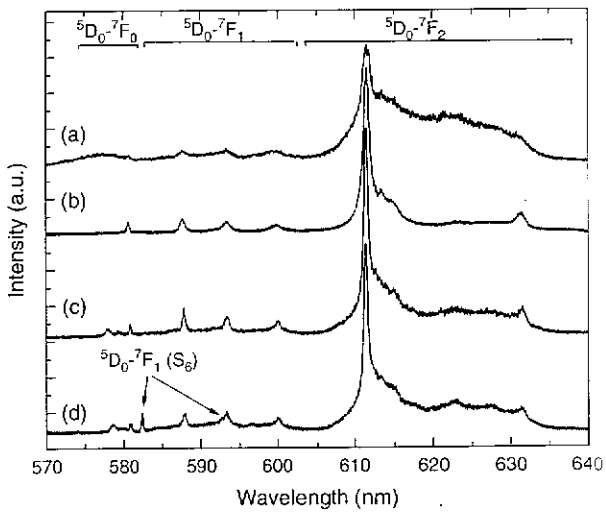

Fig. 2. Room-temperature emission spectra of the nanolayers of Eu^{3+}:Y_2O_3/Al_2O_3 by site-selective excitation at (a) λ_{exc} = 355 nm; (b) λ_{exc} = 533.55 nm; (c) λ_{exc} = 525.97 nm; and (d) λ_{exc} = 526.41 nm. Reprinted with permission from [44], X. Y. Chen et al., Nanotechnology Focus, edited by E. V. Dirote, Nova Science Publishers, New York (**2005**), p. 141. © 2005, Nova Science Publishers, Inc.

nanolayers are identified by low-temperature fluorescence spectra from $^5D_0$ and $^5D_1$. Most of the observed energy levels in nanocrystals are in good agreement with previous assignment to the bulk Y_2O_3 crystals,[56, 57] indicating that the localized electronic states remain nearly unchanged.

The excitation wavelength at 533.55 nm in Figure 2(b) corresponds to the transition from the first crystal-field (CF) level of $^7F_1$ to $^5D_1$ for Eu^{3+} ions occupying the C_2 site. This will selectively excite only the C_2 site; therefore it shows a distinct emission pattern of Eu^{3+} at the C_2 site. Figure 2(c) shows the typical spectra of overwhelming C_2 site and other minor sites even when the laser wavelength is tuned away from the resonant transition of Eu^{3+} at C_2 site. The excitation at 526.41 nm induces resonant transition from $^7F_0$ to $^5D_1$ of Eu^{3+} ions at S_6 site of the same cubic structure. For the S_6 site, only magnetic-dipole transition such as $^5D_0 \rightarrow {}^7F_1$ of Eu^{3+} is allowed. Due to energy transfer from the S_6 site to C_2 site, the emission spectrum originates mainly from C_2 site when the laser is tuned to excite the Eu^{3+} ions at S_6 site. Despite their weak intensities, two peaks from S_6 site are still observable, as marked by the arrows in Figure 2(d).

Fluorescence lifetimes of Eu^{3+} ions in nanolayers have been measured at 3.5 K, 77 K, and room temperature (RT).[44] The lifetimes of Eu^{3+} as a function of temperature are compared with those of the bulk counterparts in Figure 3. The observed lifetime of $^5D_0$ is independent of temperature for both nanocrystals and bulk crystals, consistent with the fact that multi-phonon nonradiative relaxation from $^5D_0$ is negligibly small due to the large energy gap (12,000 cm^{-1}) between $^5D_0$ and $^7F_6$. The quenching of Eu^{3+} luminescence due to the adsorption of OH^- or water impurities on the nanoparticle surface could be excluded

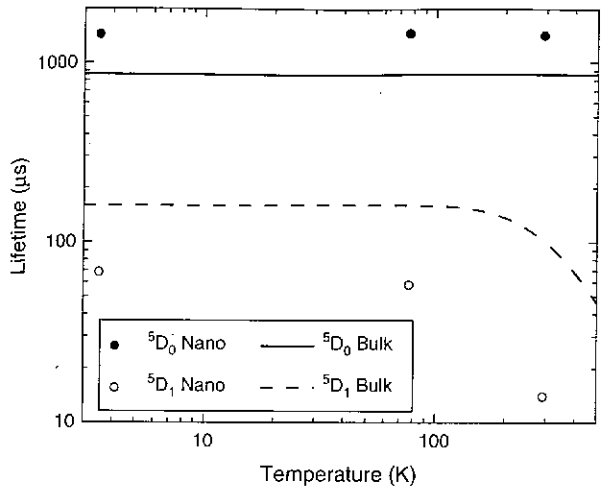

Fig. 3. Comparison of the $^5D_0$ and $^5D_1$ fluorescence lifetimes of Eu^{3+} between the core–shell Al_2O_3/Y_2O_3:Eu^{3+} and bulk Eu:Y_2O_3 crystal. Reprinted with permission from [44], X. Y. Chen et al., Nanotechnology Focus, edited by E. V. Dirote, Nova Science Publishers, New York (**2005**), p. 141. © 2005, Nova Science Publishers, Inc.

since the sample was annealed at 750 °C for 12 h. Therefore, the observed lifetime can be regarded as the radiative lifetime. The radiative lifetime of $^5D_0$ in the nanolayer of cubic Y_2O_3 (1.42 ms) was found to be unusually longer than that of the bulk counterparts (0.86 ms). The longer lifetime of $^5D_0$ in the Eu^{3+}:Y_2O_3 nanolayer is most likely due to the non-solid medium surrounding the nanoparticles that changes the effective index of refraction. The filling factor, showing what fraction of space is occupied by the Eu^{3+}:Y_2O_3 nanocoating particles, is estimated to be approximately 72% by utilizing:[11]

$$n_{\text{eff}}(x) = xn_{\text{NP}} + (1-x)n_{\text{med}} \quad (1)$$

On the other hand, the $^5D_1$ lifetime is very sensitive to temperature, since it is closely related to the multiphonon relaxation process from $^5D_1$ to $^5D_0$. When the temperature varies from 3.5 K to 295 K, the lifetime of $^5D_1$ for nanocrystals is significantly shortened from 68 μs to 13 μs. As shown in Figure 3, the lifetime of $^5D_1$ at a specific temperature for the nanocrystals is much shorter than that of the bulk counterparts, which may be attributed to concentration-induced cross relaxation between the transitions of $^5D_1 \rightarrow {}^5D_0$ and $^7F_3 \leftarrow {}^7F_0$.[58] The Eu^{3+} concentration in nanolayers is approximately 2.5 at%, higher than in the bulk, which thus accelerates the above cross relaxation.

2.1.2. *ZnO Nanoparticles as Cores*

Homogeneous Eu^{3+}:Y_2O_3 (5 at%) nanolayers (12–14 nm) coated on ZnO nanoparticles have been obtained by urea-aided hydrolysis, the annealing temperature for which (600 °C) was much lower than that for Al_2O_3 (750 °C). The HRTEM images of an uncoated ZnO nanoparticle and a coated ZnO nanoparticle are compared in Figure 4.

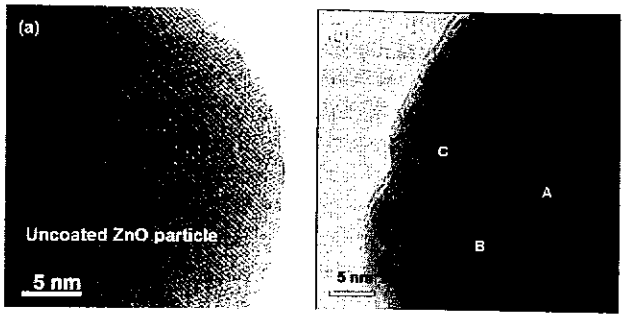

Fig. 4. HRTEM image of (a) uncoated ZnO nanoparticles; (b) ZnO nanoparticles coated with Eu^{3+}:Y_2O_3 using urea-aided hydrolysis. Reprinted with permission from [44], X. Y. Chen et al., Nanotechnology Focus, edited by E. V. Dirote, Nova Science Publishers, New York (**2005**), p. 141. © 2005, Nova Science Publishers, Inc.

It shows that the thickness of the coating layer for the selected nanoparticle is approximately 12–14 nm. The crystalline ZnO atomic lattice alignment in the uncoated nanoparticle is apparent in Figure 4(a), in accordance with the XRD analyses. The crystalline Y_2O_3 lattice in the nanolayer of the coated nanoparticle is also clearly seen in Figure 4(b). The compositions of three spots marked by A, B, and C within a nanoparticle in Figure 4(b) are further examined by energy dispersive X-ray spectrum (not shown). It turns out that the concentrations of Y and Eu elements increase from the core (A) to the nanolayer (C), whereas the concentration of Zn decreases. The XRD spectrum shows two kinds of crystalline phases, with a broad set of lines for cubic Y_2O_3 and a narrow set of lines for hexagonal ZnO.

The site-selective emission spectra are shown in Figure 5. It confirms that the nanolayers are homogeneous and primarily composed of cubic Y_2O_3 crystalline

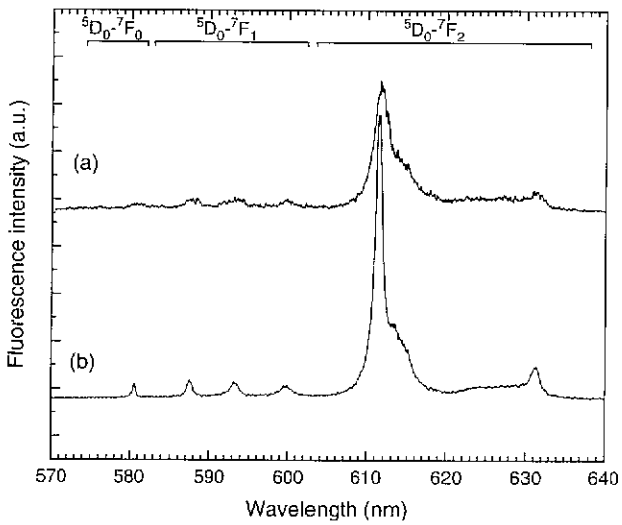

Fig. 5. Room-temperature emission spectra of the core–shell ZnO/Y_2O_3:Eu^{3+} by selective excitation at (a) λ_{exc} = 355 nm; and (b) λ_{exc} = 533.55 nm. Reprinted with permission from [44], X. Y. Chen et al., Nanotechnology Focus, edited by E. V. Dirote, Nova Science Publishers, New York (**2005**), p. 141. © 2005, Nova Science Publishers, Inc.

structures. The sharp emission peaks arising from Eu^{3+} in this sample are exactly the same as that of Eu^{3+}:Y_2O_3 coated on the Al_2O_3 core when Eu^{3+} ions at C_2 site are selectively excited at 533.55 nm. The emission pattern obtained by an ultraviolet (UV) laser excitation (Fig. 5(a)) is similar to Figure 5(b), but with much weaker intensity. This similarity shows very good homogeneity of the coating layer, while the decreased line intensity may indicate weak energy transfer between the ZnO core and nearby Eu^{3+} ions at higher excited states.

Similar to the core–shell of Al_2O_3/Y_2O_3:Eu^{3+} nanocomposites, the decay from $^5D_0$ of Eu^{3+} in ZnO/Y_2O_3:Eu^{3+} (Fig. 6) fits well to a single exponential, indicating a homogeneous environment around Eu^{3+}. The longer lifetime (1.84 ms) of $^5D_0$ in ZnO/Y_2O_3:Eu^{3+} is also attributed to the change of the effective index of refraction as stated before. The filling factor is estimated to be approximately 58%, smaller than that of Al_2O_3/Y_2O_3:Eu^{3+} (72%). The much shorter $^5D_1$ lifetime (27 μs at RT) than the bulk counterpart (90–120 μs) is related to the enhanced nonradiative multiphonon relaxation induced by surface effects or concentration quenching in nanocrystals. It is noteworthy that the optical properties of ZnO cores are not affected after the nanocoating process. The observed emission spectra in UV region from ZnO cores are the same as that of ZnO uncoated nanoparticles.

2.2. Crystallization and Nanophase Transition

Interesting crystallization and phase transition phenomena have been observed in the as-grown Al_2O_3/Y_2O_3:Eu^{3+} core–shell nanophosphors prepared by the ammonia-aided hydrolysis method.[43] It is shown that the coated films of the nanophosphors crystallize at temperatures higher than 600 °C and may be completely converted into cubic Y_2O_3 nanocrystalline layers at 750 °C. At 900 °C, phase transition occurs across the boundary between the outer coating layer and the inner core. All possible crystallographic phases, including two of solid-state laser ceramics, $YAlO_3$ (YAP), and $Y_3Al_5O_{12}$ (YAG), can be formed in the pseudobinary Al_2O_3-Y_2O_3 nanosystem by controlling the thermal annealing procedures from 600 to 900 °C, a temperature range far below the conventional solid-state reaction temperature. The experimental conditions for the above phase transition are summarized in Figure 7. Obviously, the thermodynamics for bulk systems are not applicable to nanoscale systems. This type of nanophase transition is closely related to the surface effect.[44] However, the chemical dynamics in the coating nanoparticles are rather complex and thus deserve further studies.

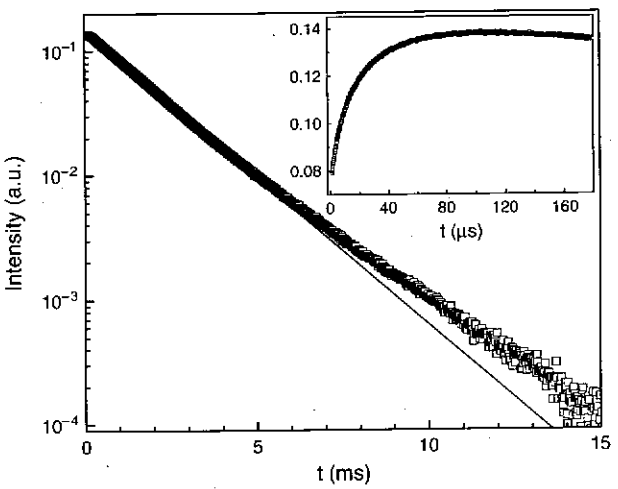

Fig. 6. Fluorescence decay from $^5D_0$ of Eu^{3+} in the core–shell ZnO/Y_2O_3:Eu^{3+} at room temperature. The inset shows the initial rise due to the decay from $^5D_1$. The line is the fit to the experimental data. Reprinted with permission from [44], X. Y. Chen et al., Nanotechnology Focus, edited by E. V. Dirote, Nova Science Publishers, New York (2005), p. 141. © 2005, Nova Science Publishers, Inc.

2.3. Dopant Site Location in Core and Core–Shell Nanoparticles

Lehmann et al. recently provided direct spectroscopic evidence to identify the dopant site location at the surface and in the interior of Eu^{3+}:$LaPO_4$ nanoparticles which were prepared in a high-boiling coordinating solvent mixture.[34] The core–shell nanoparticles belong to category I. Having compared the site-selective spectroscopy of Eu^{3+}:$LaPO_4$ nanocrystals with that of Eu^{3+}:$LaPO_4$/$LaPO_4$ core–shell nanoparticles, they concluded that surface sites could be converted completely into bulk sites by overgrowing the nanoparticles with a shell of pure $LaPO_4$.

Figure 8 shows the spectra of the Eu^{3+}:$LaPO_4$ (5%) core nanoparticles before a $LaPO_4$ shell was grown onto them. Site-selective fluorescence spectra for the excitation at 17,294, 17,286, and 17,279 cm^{-1} correspond to the L-, M-, and H-sites in the bulk counterparts, respectively. For

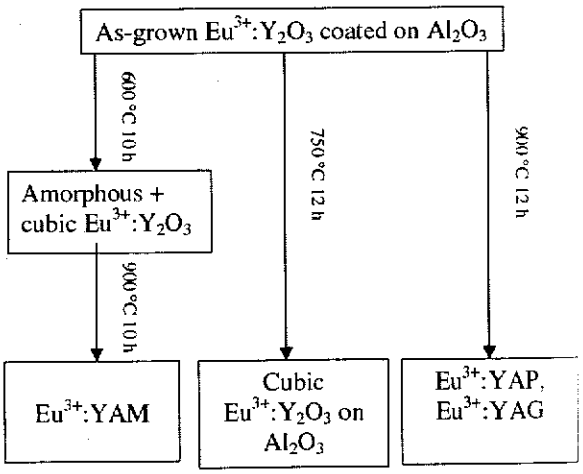

Fig. 7. Resulting crystalline phases from the thermal annealing of amorphous Eu^{3+}:Y_2O_3 films coated on Al_2O_3 nanocrystals. Reprinted with permission from [43], X. Y. Chen et al., *Nanotechnology* 14, 670 (2003). © 2003, Institute of Physics and IOP Publishing Ltd.

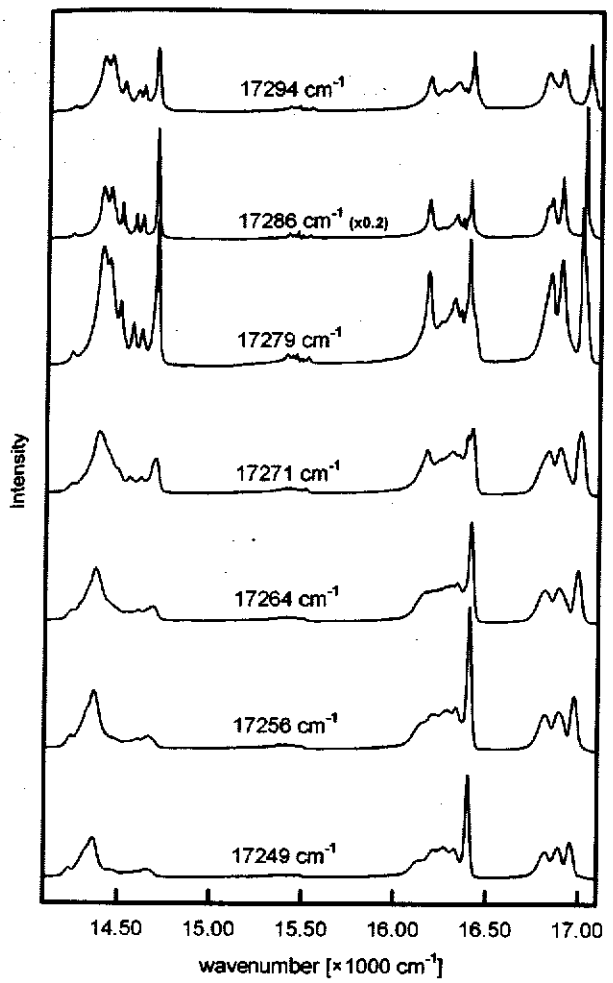

Fig. 8. Site-selective fluorescence spectra of Eu^{3+}:$LaPO_4$ (5%) nanoparticles without shells, excited at 30 K at the wave numbers indicated. Without the $LaPO_4$ shell, the Eu^{3+}:$LaPO_4$ (5%) nanoparticles display spectra of additional Eu^{3+} sites over the entire excitation range. Reprinted with permission from [34], O. Lehmann et al., *J. Am. Chem. Soc.* 126, 14935 (**2004**). © 2004, American Chemical Society.

comparison, no other sites were identified in the site-selective emission spectra of Eu^{3+}:$LaPO_4$/$LaPO_4$ core–shell nanoparticles over the whole excitation range (17,249–17,294 cm^{-1}), indicating that those three sites are located in the interior of the nanoparticles. Luminescence from additional sites with comparatively broad lines appears over the whole excitation range and has its highest emission intensity under excitation at 17,256 cm^{-1} for Eu^{3+}-doped core nanoparticles, which is absent for the core–shell counterparts. The fact that this additional emission disappears when a shell is grown onto the nanoparticle surface clearly indicates that it is related to Eu^{3+} in surface sites. To verify the origin of the surface sites, Lehmann et al. prepared $LaPO_4$ nanoparticles with Eu^{3+} ions only on their surface by reacting Eu^{3+} and phosphate ions with the surface of pure $LaPO_4$ particles in a manner similar to the procedure employed for the growth of $LaPO_4$ shells. They found that surface sites in Eu^{3+}:$LaPO_4$ nanoparticles without shells are identical to those $LaPO_4$ nanoparticles with Eu^{3+} on their surface, having the same site-selective emission spectra. They also verified that additional Eu^{3+} sites in Eu^{3+}:$LaPO_4$ core nanoparticles are not the same Eu^{3+} sites of $EuPO_4$ particles that nucleated in solution separately from the doped $LaPO_4$ nanoparticles, based on the fact that the site-selective luminescence spectra of the small (or large) $EuPO_4$ particles are significantly different from those of the $LaPO_4$/surface Eu^{3+} and Eu^{3+}:$LaPO_4$ nanoparticles.

The fluorescence lifetimes of the major site (M-site) and the surface site of Eu^{3+} (5%) in $LaPO_4$ nanoparticles without a shell were measured to be 3.7 ms and 1.6–2.3 ms (multi-exponential decay) at 30 K, respectively.[34] Compared to the lifetime of bulk counterparts (3.18 ms),[59] the former is slightly prolonged while the latter is significantly shortened. It is not surprising that a shorter lifetime is observed for the surface sites, because the proximity to high-energy vibrations of organic ligands may quench the luminescence of Eu^{3+}. The fluorescence lifetime of the M-site in Eu^{3+}:$LaPO_4$/$LaPO_4$ core–shell nanoparticles was measured to be 4.2 ms, which is slightly longer than that of the sample without shell, a convincing evidence of improving quantum efficiency. Hence, the core–shell technique allows one to prepare doped nanoparticles that contain no other dopant sites than those known from the corresponding bulk material, despite their small size less than 15 nm. The quantum efficiency of RE ions can also be improved by virtue of the surface modification of nanoparticles.

2.4. Core–Shell Structure with Tunable Thickness of Shells

To obtain monodisperse spherical core–shell structured phosphors for field emission displays (FED), Wang et al. synthesized SiO_2/Y_2O_3:Eu^{3+} core–shell particles by a Pechini sol–gel process.[51] It has been demonstrated that the thickness of Eu^{3+}:Y_2O_3 shell could be easily controlled by changing the number of deposition cycles (e.g., 60 nm for three deposition cycles). The SiO_2/Y_2O_3:Eu^{3+} core–shell particles (coated three times) showed a strong red emission typical of Eu^{3+} under the UV excitation at 250 nm or low-voltage electron beams (2–6 kV). The photoluminescence (PL) and cathodoluminescence (CL) intensity of SiO_2/Y_2O_3:Eu^{3+} core–shell phosphors are also tunable and depend on the number of the coatings or the thickness of the Eu^{3+}:Y_2O_3 shells on the SiO_2 cores (500 nm). The increase in the thickness of Eu^{3+}:Y_2O_3 shells results in an increase in PL intensity of Eu^{3+}. It is observed that the PL intensity of four-layer Eu^{3+}:Y_2O_3-coated SiO_2 core–shell phosphors could reach about 80% that of the pure Eu^{3+}:Y_2O_3 prepared in a similar process.[51] Similarly, the thickness of the Eu^{3+}:YVO_4 (or $CaWO_4$) shells on SiO_2 cores could also be tailored by varying the number of deposition cycles.[50, 52] For SiO_2/YVO_4:Eu^{3+} core–shell particles (60 nm for two deposition cycles), a

strong PL dominated by $^5D_0 \rightarrow {}^7F_2$ red emission at 617 nm is observed due to an efficient energy transfer from the vanadate groups to the Eu^{3+}. The PL intensity of a four-layer Eu^{3+}:YVO_4-coated SiO_2 core–shell phosphor has reached about 70% that of the pure Eu^{3+}:YVO_4 powder phosphor. The above core–shell technique may lower the cost of the final phosphors due to the partial substitution of the cheaper silica for the expensive RE materials.

3. HOLLOW NANOSPHERES

Monodisperse hollow nanospheres containing RE ions have various potential applications such as high-resolution imaging and displays and biolabels due to their large surface areas and hollow characteristics. The luminescence intensity of RE-doped hollow nanophosphors could reach the same level as that of the solid nanoparticles without any compromise, while raw materials are significantly saved in synthesis of hollow nanophosphors. Wang et al. reported the synthesis of Eu^{3+}-doped Y_2O_3, YOF, La_2O_3, and LaOF hollow nanospheres by a sonochemical assisted template route, in which the size of the hollow spheres could be tailored by selecting different sized carbon sphere templates.[60] Emission spectra of Eu^{3+} doped into Y_2O_3, YOF, La_2O_3, and LaOF hollow spheres have shown dominant $^5D_0 \rightarrow {}^7F_2$ red emissions, similar to their bulk counterparts. However, no detailed spectroscopy including lifetime behavior has been reported for this type of materials. The carbon sphere templates used by Wang et al. are in the submicron range. Liu et al. synthesized hollow Eu^{3+}:Y_2O_3 nanospheres (20 nm shell thickness) by etching the SiO_2/Y_2O_3:Eu^{3+} core–shell nanoparticles with NaOH solution.[61] No significant difference in emission spectrum has been observed for either the hollow nanospheres or their core–shell counterparts.

Interestingly, a series of LnF_3 (Ln = Y, La, Pr, Nd, and Sm) and $Ln(OH)_3$ (Ln = Y, Sm, Eu, Gd, Tb, Dy, Ho, and Er) fullerene-like nanoparticles have been successfully synthesized based on a low-temperature (80–180 °C) hydrothermal method.[62] Wang and Li observed that the formation of fullerene-like nanoparticles was closely related to the hexagonal structures of the corresponding samples, since comparatively fewer fullerene-like nanoparticles were observed in the samples of orthorhombic YF_3 and no fullerene-like nanoparticles were observed in the orthorhombic samples of other LnF_3 (Ln = Eu, Gd, Tb, Dy, Ho, Er, Tm, Yb, and Lu). The hydroxide fullerene-like nanoparticles usually coexist with nanotubes in final products. The hollow sphere nature of these samples has been further confirmed through BET surface area measurement, since those samples exhibit a larger surface area than the non-hollow bulk crystals. The size of hollow spheres can also be tuned by controlling the hydrothermal temperature. For example, the average diameter of PrF_3 fullerene-like nanoparticles synthesized at 120 °C is 10 nm, while it increases to 30–50 nm for the same materials synthesized at 180 °C. So far no optical properties of these materials have been reported. The luminescence dynamics of RE doped hollow nanospheres with a size of 1–10 nm is expected to be very distinct compared to their bulk ones or solid nanoparticles, thus deserves further study in the future.

4. NANOTUBES AND NANOWIRES

The optical properties of RE ions in some 1D nanomaterials may behave differently from those of 0D nanoparticles and bulk materials. Recently we observed a significantly long lifetime of $^5D_0$ and reported experimental evidence of anomalous thermalization in Eu^{3+}:Gd_2O_3 nanotubes (NTs).[63] Figure 9 shows the TEM image of the Eu^{3+}:Gd_2O_3 (4 at%) NTs prepared via a hydrothermal method. The NTs have an average diameter of ~20 nm, wall thickness of ~5 nm and lengths of 70–80 nm. XRD results confirm its cubic crystalline phase. Interestingly, we observed an anomalous thermalization effect in Gd_2O_3:Eu^{3+} NTs at 10 K. Hot bands originated from the CF level of $^7F_1$ with an energy of 217 cm^{-1} appear in the 10 K excitation spectrum as shown in Figure 10(a). According to the Boltzmann distribution of Eu^{3+} population, Eu^{3+} ions should populate only the lowest level $^7F_0$ at 10 K, and no population should be accumulated at $^7F_1$ due to very fast phonon relaxation to the ground state. Hence under normal conditions, the excitation spectrum is expected to be exactly like that of the bulk sample without detectable excitation peaks arising from level $^7F_1$. However, as shown in the long-wavelength side of Figure 10(a), two hot bands assigned to the transitions from the lowest level of $^7F_1$ to the two CF levels of $^5D_1$ (18,944 and 18,962 cm^{-1}) are observed. Similar

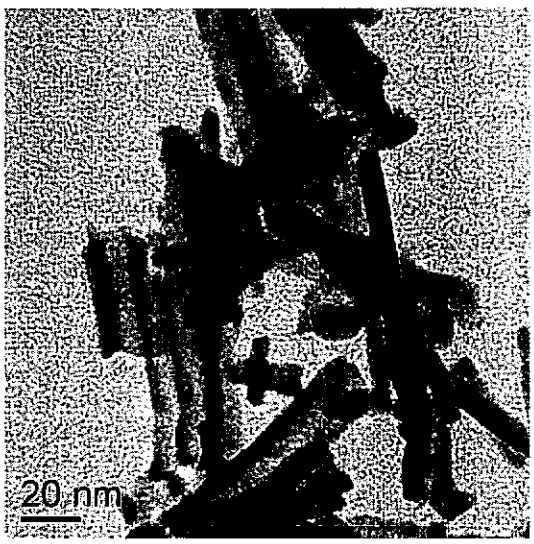

Fig. 9. TEM images of Eu^{3+}:Gd_2O_3 nanotubes. Reprinted with permission from [63], L. Q. Liu et al., *Nanotechnology* 18, 015403 (2007). © 2007, Institute of Physics and IOP Publishing Ltd.

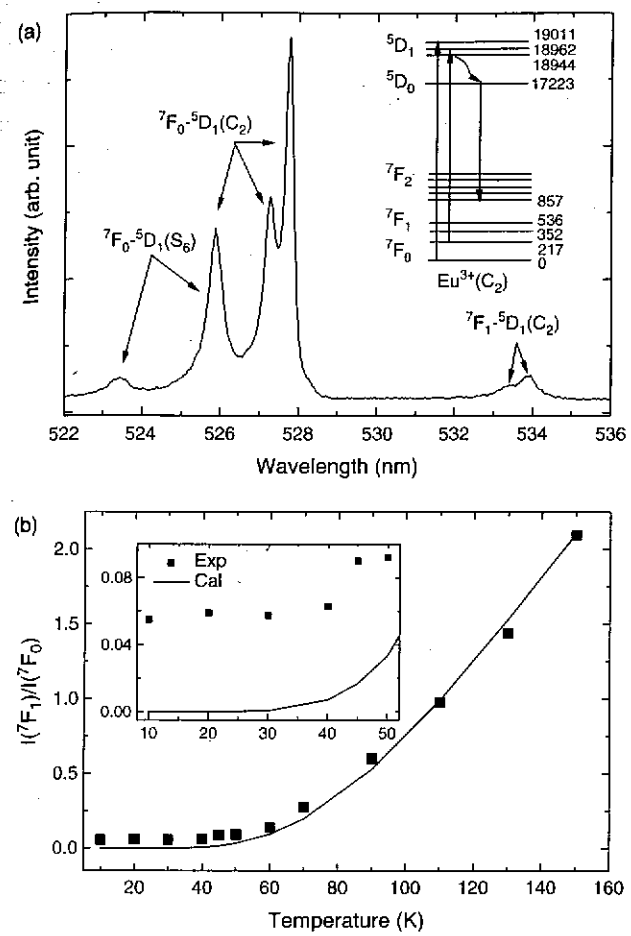

Fig. 10. (a) Excitation spectrum of Eu^{3+}:Gd_2O_3 nanotubes in the region of $^7F_0$-$^5D_1$ at 10 K, monitoring the $^5D_0 \rightarrow {}^7F_2$ (C_2) emission at 611.0 nm. The schematic diagram of partial energy levels of Eu^{3+} ions is presented. (b) Temperature dependence of the integrated intensity ratio of the hot bands to normal bands in (a), $I(^7F_1)/I(^7F_0)$. The scattering dots are observed ones, whereas the line denotes the calculated values based on the Boltzmann distribution. Reprinted with permission from [63], L. Q. Liu et al., *Nanotechnology*.18, 015403 (**2007**). © 2007, Institute of Physics and IOP Publishing Ltd.

phenomenon has been reported for Er^{3+} in Y_2O_2S nanocrystals where hot bands originating from the upper CF levels of $^4I_{15/2}$ with an energy gap up to 224 cm^{-1} were observed in the excitation spectra at 2.6 K.[14] Due to the large energy gap between $^7F_1$ and $^7F_0$, the intensities of the observed hot bands in Gd_2O_3:Eu^{3+} NTs were much weaker than the normal bands. According to the theoretical model proposed by Liu et al.,[13,14] this anomalous thermalization is likely due to the restricted phonon relaxation in NTs. It is well-known that the phonon density of states (PDOS) is discrete and the low-frequency acoustical phonon modes are cut off in nanocrystals.[14,64,65] Therefore nonradiative phonon relaxation of ions in certain electronically excited states is expected to be different from that in bulk materials. Presumably the morphology of 1D nanostructures such as NTs would have distinct PDOS in which the low-energy acoustical phonon modes are significantly cut off. It was roughly estimated that the PDOS around 217 cm^{-1} become discrete and are reduced to some extent in views of the one-dimensional confinement (perpendicular to the wall, with a thickness of ~5 nm). Nevertheless theoretical calculation of the phonon spectrum for the 1D nanosystems is required for better understanding the above relaxation dynamics. The intensity of the hot bands hardly changes below 50 K but increases and exhibits normal Boltzmann thermalization above 60 K, as shown in Figure 10(b). This behavior can be interpreted based on a competition model similar to the case of Er^{3+}:Y_2O_2S.[13] The equilibrium population in the lowest sublevel of $^7F_1$ results from the competition between the light-induced thermalization (populating process) and the restricted direct phonon relaxation (depopulating process). The populating rate of the light-induced thermalization is proportional to the rate of multiphonon relaxation from $^5D_1$ to $^5D_0$ where four phonons of 430 cm^{-1} are required to bridge the gap. At low temperature (below 50 K), this multi-phonon relaxation rate and the phonon occupation number $[\exp(217/0.695T) - 1]^{-1}$ for one phonon process are both weakly dependent on the temperature, therefore the relative population in the 217 cm^{-1} sublevel of $^7F_1$ is insensitive to the temperature.[63]

Furthermore, the fluorescence lifetime of $^5D_0$ (2.19 ms at 10 K) in Eu^{3+}:Gd_2O_3 NTs is found to be much longer than that of the bulk counterparts (0.94 ms), indicating a small filling factor of 0.55 for the NTs. Similarly, the lifetime of $^5D_0$ in Eu^{3+}:Y_2O_3 NTs with diameters of 20–40 nm, length of ~1 μm and wall thickness of 5–10 nm was measured to be 1.36 ms,[66] which is also longer than their bulk counterparts (0.9 ms), corresponding to a filling factor of 0.74. The more remarkable lifetime lengthening in Gd_2O_3 NTs than in Y_2O_3 NTs could be interpreted in view of the different morphologies between the two samples. The smaller diameter, wall thickness, and length of the former may result in a smaller filling factor (or effective index of refraction) thus longer radiative lifetime.

The luminescence dynamics of RE in nanotubes and nanowires may also behave very differently. For instance, nanowires (NWs) of Eu^{3+}:$LaPO_4$ phosphors were synthesized by the hydrothermal method with a diameter of 10–20 nm and a length of several hundred nanometers.[8–10] Site selective fluorescence spectra indicate that Eu^{3-} ions occupied an additional site besides the main site observed in nanoparticles and microcrystals. The luminescent quantum efficiency of the $^5D_1 \rightarrow {}^7F_J$ transitions of Eu^{3+} in $LaPO_4$ NWs, reaching 59%, is remarkably enhanced compared to that of the corresponding nanoparticles (38%), micrometer particles (47%) and micrometer rods (49%). Interestingly, the radiative transition rate from $^5D_1$ (or $^5D_0$) of Eu^{3+} in NWs could increase at least 1.5 times over that in nanoparticles and microcrystals. Obviously, this shortened radiative lifetime in NWs cannot be explained by the correction of effective refraction of index as discussed

before, which otherwise results in a lengthened radiative lifetime. Yu et al. attributed the increase of the radiative electronic transition rate in NWs to the variation of electric or magnetic-dipole field caused by the shape anisotropy.[10] In a subsequent paper, Yu et al. observed a shorter radiative lifetime of $^5D_0$ with the increasing ratio of length to width (LWR) for Eu^{3+}:$LaPO_4$ NWs. That is, the lifetime of $^5D_0$ decreased from 2.41 ms to 1.70 ms when the LWR of the NWs increased from 10 to 30.[67] This trend is in accordance with the above assumption since a large LWR corresponds to larger shape anisotropy. However, no similar trend has been observed for cubic Eu^{3+}:Y_2O_3 NTs and NWs synthesized through a similar hydrothermal method at various temperatures.[66] The nanocrystals prepared at 130 °C yielded NTs with wall thickness of 5–10 nm and outer diameter of 20–40 nm. The nanocrystals prepared at 170 and 180 °C yielded NWs with diameters of ~100 and ~300 nm, respectively. The radiative lifetime of $^5D_0$ was determined to be 1.36 ms in NTs, 1.91 ms in 100-nm NWs, and 1.65 ms in 300-nm NWs, significantly larger than that in bulk counterparts (0.9 ms). Therefore more evidence, including a sound theoretical model, is required to establish the relationship between the shape anisotropy and the observed radiative lifetime.

Bai et al. observed a phonon sideband with a frequency shift of 40–50 cm^{-1} located at the low-energy side of the $^7F_0 \rightarrow {}^5D_0$ zero-phonon line (ZPL) in the 77 K excitation spectra of Eu^{3+}:Y_2O_3 NTs and NWs.[66] Curiously, vibronic sidebands generally appear at the high-energy side of the ZPL in low-temperature excitation spectra since the vibronic transition involving the creation of a phonon with the annihilation of a photon is much more favored than the annihilation of a phonon at low-temperature. The origin of this sideband is not yet clear.

Wang et al. observed that NTs of lighter lanthanide hydroxide compounds with smaller diameters could be synthesized by the hydrothermal method, while those of heavier lanthanide hydroxides were obtained with larger diameters under similar experimental conditions.[68] For example, NTs of $Ln(OH)_3$ (Ln = Y, Yb, Tm, Er, Ho, Dy, and Tb) have diameters from around tens of nanometers to more than one hundred nanometers, while those of light Ln [Ln = Gd, Eu, Sm, Nd, Pr, and La, (all before Gd in the periodic table)] have diameters less than 20 nm. They attributed this difference to the gradual changes of the radii of the Ln ions and the crystal-field changes. Interestingly, these NTs with open ends show excellent hydrophilic properties, which provide a possibility of wetting processing in the inner parts with capillary action as the driving force. These NTs can also be further chemically modified to form RE-doped oxysulfide NTs. Excitation and emission spectra of Eu^{3+}:Y_2O_2S NTs have shown typical S^{2-}-Eu^{3+} charge-transfer band and emission lines of Eu^{3+} respectively. However the assignment of Er^{3+} emission bands in the upconversion and down-conversion spectra of Er^{3+}, Yb^{3+}:Y_2O_2S NTs is questionable since either spectrum did not exhibit the typical emission lines of Er^{3+} as observed in other similar nanocrystals.[68]

5. NANOSHEETS, NANODISKS AND OTHERS

Recently, optical spectra of RE doped in some other novel nanostructures such as nanosheets and nanodisks have occasionally been reported.[69–72] Si et al. developed a nonhydrolytic synthetic route to prepare high-quality dispersible RE oxide nanocrystals including nanopolyhedra, ultrathin nanodisks, and nanoplates, which exhibit striking self-assembly capabilities into large area nanoarrays.[70, 71] Particularly, high-quality cubic phase Eu^{3+}:Y_2O_3 nanodisks were obtained via simultaneous thermolysis of multiple RE acetylacetonates in the mixed solvent of oleic acid/oleylamine/1-octadecene, in which there exists a Eu^{3+} site not present in its bulk counterparts. The size of the Eu^{3+}:Y_2O_3 nanodisks could be tuned from 16.0 to 23.2 nm. Figure 11 compares the RT fluorescence spectra of four Eu^{3+}:Y_2O_3 samples (Y1, 16.0 nm nanodisk; Y2, 23.2 nm nanodisk; Y3, 40 nm nanoparticle prepared by a coprecipitation method; Y4, commercial powder). As shown in Figure 11(a) (right part), the bands in the wavelength of 560–720 nm can be described as the $^5D_0 \rightarrow {}^7F_J$ line emissions ($J = 0$, 1, 2, 3, and 4) of the Eu^{3+} ion, and the nearly same Eu^{3+} luminescence patterns are observed for both Y3 and Y4, which show no obvious size effect. Very different emission patterns are observed for the nanodisks Y1 and Y2. In comparison with the nanoparticle Y3 and bulk Y4 references, the emission lines of Y1 and Y2 are significantly broadened as a result of size reduction. The charge-transfer bands of the nanodisks Y1 and Y2, as shown in the UV excitation spectra in Figure 11(a) (left part), are distinctly red-shifted, possibly due to the capped oleylamine ligand on the nanodisk surface that could result in an enhanced covalent bonding. Most strikingly, a new peak around 625 nm appears in the $^5D_0 \rightarrow {}^7F_2$ emission spectrum for Eu^{3+} in the nanodisks Y1 and Y2. This new peak is slightly blue-shifted from the 631-nm peak that is assigned to Eu^{3+} at the C_2 site for bulk crystals. Site-selective laser excitation spectra have further confirmed the existence of a new site of Eu^{3+} for the Y2 nanodisks. As shown in Figure 11(b), the peak located at 580.7 nm is assigned to the $^5D_0 \rightarrow {}^7F_0$ transition for the cubic bulk reference, whereas the peak at 581.1 nm is ascribed to the emerging site due to the ultrathin thickness of the nanodisk. The appearance of new Eu^{3+} site in the ultrathin nanodisks is closely related to its distinct surface structure. Similarly, the nanofilms of cubic Eu^{3+}:Y_2O_3 with thickness less than 20 nm have been prepared by pulsed laser deposition and exhibit a completely different crystal-field environment from that of bulk counterparts with thickness of 100–500 nm.[7] Luminescence from the

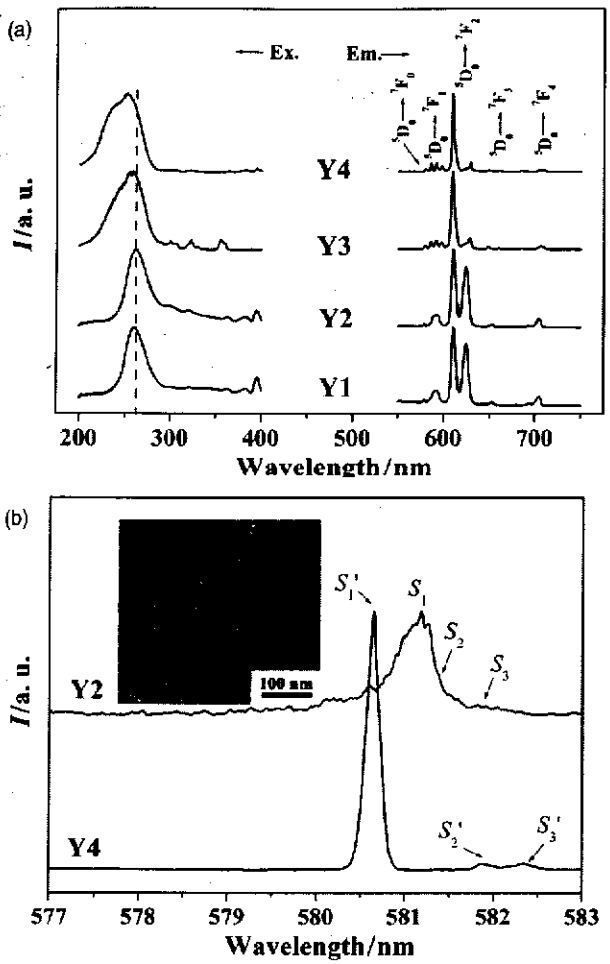

Fig. 11. (a) RT fluorescence spectra of the Eu^{3+}:Y_2O_3 (5 at%) samples: Y1, 16.0 nm nanodisk ($\lambda_{em} = 612$ nm, $\lambda_{ex} = 263$ nm); Y2, 23.2 nm nanodisk ($\lambda_{em} = 610$ nm, $\lambda_{ex} = 263$ nm); Y3, 40 nm nanoparticle prepared by a coprecipitation method ($\lambda_{em} = 610$ nm, $\lambda_{ex} = 260$ nm); Y4, commercial powder ($\lambda_{em} = 610$ nm, $\lambda_{ex} = 253$ nm). (b) Site-selective laser excitation spectra of Y2 and Y4 by monitoring the 625 and 610 nm emission at 77 K, respectively. The inset shows the TEM image of the Y2 nanodisks. Reprinted with permission from [71], R. Si et al., *Chem. Mater.* 19, 18 **(2007)**. © 2007, American Chemical Society.

new site of Eu^{3+} in cubic Gd_2O_3 nanocrystals prepared by a sol-lyophilization technique has also been reported.[5]

Wang et al. showed that well-dispersed Eu^{3+}:Y_2O_3 nanocrystals could be prepared via a non-hydrolic route at very low temperature (230 °C).[73] Eu^{3+}:Y_2O_3 nanodisks could be synthesized under higher reaction temperature (>270 °C) without the addition of trioctylphosphine oxide. The nanodisks would be self-assembled to form one to three dimensional structures under different reaction times. Jiang et al. synthesized uniform donut-like assemblies of Eu^{3+}:YBO_3 via a simple hydrothermal method in the absence of any surfactant or template.[74] These microparticles are actually composed of orderly aggregated nanosheets and exhibit improved chromaticity compared with the bulk or the sample calcinated at high temperatures. This improvement of chromaticity (higher red/orange ratio in the emission) is ascribed to the distinct building blocks—nanosheets with large surface area and high surface energy—which result in a high degree of disorder and lower CF symmetry around the Eu^{3+} ions.

As for the synthesis method of novel nanostructures, Wang et al. have developed a general strategy for the fabrication of a series of functional nanocrystals with different chemistries and properties including noble metal, magnetic/dielectric, semiconducting, RE fluorescent, biomedical, organic optoelectronic semiconducting, and conducting polymer nanoparticles.[75] This method is developed based on a general phase transfer and separation mechanism occurring at the interfaces of the liquid-solid solution (LSS) phases present during the synthesis. In particular, LSS phase transfer and separation approach have been successfully applied to synthesize nearly monodisperse RE fluorescent nanocrystals. The synthesized $NaYF_4$, YF_3, LaF_3 and YbF_3 nanoparticles are spherical with diameters of 4–12 nm. The YF_3 nanoparticles have a ricelike shape with a diameter of 100 nm and length of 500 nm (composed of uniform nanocrystals with a diameter of 5 nm). The $Ln(OH)_3$ nanoparticles are composed of uniform nanorods with a diameter 3–15 nm. By doping with different RE ions these nanocrystals can be functional as nanophosphors. Green upconversion of Yb/Er co-doped $NaYF_4$ nanocrystals has been demonstrated when excited with a 980 nm laser. Therefore, this LSS strategy is very important which provides a simple and convenient route to prepare abundant novel nanostructures containing RE ions for many potential applications.

6. CONCLUSIONS

Research and development of nanoscale luminescent and laser materials are part of the rapidly advancing nanoscience and nanotechnology. Doping luminescent RE ions into nano-hosts is an ideal approach to developing nano-devices for various applications. For example, coating of RE nanophosphors on blue LEDs for white light emission is currently considered for future energy-saving lighting devices to replace the fluorescent lamps. Research on doping of luminescent RE ions into semiconductor nanocrystals may lead to the advent of a new series of highly efficient luminescent materials. We have reviewed in this article the most recent progress in optical spectroscopy of novel low-dimensional nanostructures such as nanolayers, core–shells, nanowires, nanotubes, hollow nanospheres, and nanodisks. The relationship between their unique structures and optical properties is discussed, and their unique spectroscopic properties and luminescence dynamics are highlighted. It is anticipated that the combination of the distinct optical properties of RE ions and novel nanostructures will create a variety of such technological applications as fabrication of optoelectronic devices, flat panel displays, and nanoscale biosensors.

Acknowledgment: This work is supported by the Knowledge Innovation and One Hundred Talents Programs of the Chinese Academy of Sciences, the NSFC (Grant Nos. 10504032 and 10774143), the 973 program (No. 2007CB936703), the Startup Foundation from the State Ministry of Personnel of China, and the Science and Technology Foundation of Fujian Province (Nos. 2006F3137 and 2007I0024). Work at Argonne National Laboratory was supported by the U.S. Department of Energy, Office of Basic Energy Sciences, Division of Chemical Sciences, Geosciences, and Biosciences, under contract DE-AC02-06CH11357.

References and Notes

1. B. M. Tissue, *Chem. Mater.* 10, 2837 (**1998**).
2. P. A. Tanner, *J. Nanosci. Nanotechnol.* 5, 1455 (**2005**).
3. P. N. Prasad, Nanophotonics, John Wiley & Sons, New York (**2004**).
4. G. K. Liu and X. Y. Chen, Handbook on the Physics and Chemistry of Rare Earths, edited by K. A. Gschneidner, Jr., J. C. G. Bunzli, and V. K. Pecharsky, Elsevier Science B.V., Amsterdam (**2007**), Vol. 37, p. 99.
5. B. Mercier, C. Dujardin, G. Ledoux, C. Louis, O. Tillement, and P. Perriat, *J. Appl. Phys.* 96, 650 (**2004**).
6. C. F. Wu, W. P. Qin, G. S. Qin, D. Zhao, J. S. Zhang, S. H. Huang, S. Z. Lu, H. Q. Liu, H. Y. Lin, and R. Tenne, *Appl. Phys. Lett.* 82, 520 (**2003**).
7. S. Bar, G. Huber, J. Gonzalo, A. Perea, A. Climent, and F. Paszti, *Mat. Sci. Eng. B-Solid* 105, 30 (**2003**).
8. H. W. Song, L. X. Yu, S. Z. Lu, Z. X. Liu, L. M. Yang, and T. Wang, *Opt. Lett.* 30, 483 (**2005**).
9. H. W. Song, L. X. Yu, S. Z. Lu, T. Wang, Z. X. Liu, and L. M. Yang, *Appl. Phys. Lett.* 85, 470 (**2004**).
10. L. X. Yu, H. W. Song, S. Z. Lu, Z. X. Liu, L. M. Yang, and X. G. Kong, *J. Phys. Chem. B* 108, 16697 (**2004**).
11. R. S. Meltzer, S. P. Feofilov, B. Tissue, and H. B. Yuan, *Phys. Rev. B* 60, R14012 (**1999**).
12. H. Schniepp and V. Sandoghdar, *Phys. Rev. Lett.* 89, 257403 (**2002**).
13. G. K. Liu, X. Y. Chen, H. Z. Zhuang, S. Li, and R. S. Niedbala, *J. Solid State Chem.* 171, 123 (**2003**).
14. G. K. Liu, H. Z. Zhuang, and X. Y. Chen, *Nano Lett.* 2, 535 (**2002**).
15. D. Matsuura, *Appl. Phys. Lett.* 81, 4526 (**2002**).
16. A. Patra, C. S. Friend, R. Kapoor, and P. N. Prasad, *Appl. Phys. Lett.* 83, 284 (**2003**).
17. R. X. Yan and Y. D. Li, *Adv. Funct. Mater.* 15, 763 (**2005**).
18. S. Heer, K. Kompe, H. U. Gudel, and M. Haase, *Adv. Mater.* 16, 2102 (**2004**).
19. G. S. Yi, B. Q. Sun, F. Z. Yang, D. P. Chen, Y. X. Zhou, and J. Cheng, *Chem. Mater.* 14, 2910 (**2002**).
20. G. S. Yi, H. C. Lu, S. Y. Zhao, G. Yue, W. J. Yang, D. P. Chen, and L. H. Guo, *Nano Lett.* 4, 2191 (**2004**).
21. L. Y. Wang, R. X. Yan, Z. Y. Hao, L. Wang, J. H. Zeng, H. Bao, X. Wang, Q. Peng, and Y. D. Li, *Angew. Chem. Int. Edit* 44, 6054 (**2005**).
22. F. Vetrone, J. C. Boyer, J. A. Capobianco, A. Speghini, and M. Bettinelli, *J. Phys. Chem. B* 106, 5622 (**2002**).
23. F. Vetrone, J. C. Boyer, J. A. Capobianco, A. Speghini, and M. Bettinelli, *J. Appl. Phys.* 96, 661 (**2004**).
24. L. Yang, H. Song, L. Yu, Z. Liu, and S. Lu, *J. Lumin.* 116, 101 (**2006**).
25. H. W. Song, B. J. Sun, T. Wang, S. Z. Lu, L. M. Yang, B. J. Chen, X. J. Wang, and X. G. Kong, *Solid State Commun.* 132, 409 (**2004**).
26. Y. Q. Lei, H. W. Song, L. M. Yang, L. X. Yu, Z. X. Liu, G. H. Pan, X. Bai, and L. B. Fan, *J. Chem. Phys.* 123, 174710 (**2005**).
27. G. S. Yi and G. M. Chow, *Adv. Funct. Mater.* 16, 2324 (**2006**).
28. G. S. Yi and G. M. Chow, *Chem. Mater.* 19, 341 (**2007**).
29. R. S. Meltzer, W. M. Yen, H. R. Zheng, S. P. Feofilov, M. J. Dejneka, B. M. Tissue, and H. B. Yuan, *Phys. Rev. B* 6410, 100201 (**2001**).
30. R. S. Meltzer, W. M. Yen, H. R. Zheng, S. P. Feofilov, and M. J. Dejneka, *Phys. Rev. B* 66, 224202 (**2002**).
31. E. Ma, Z. J. Hu, Y. S. Wang, and F. Bao, *J. Lumin.* 118, 131 (**2006**).
32. K. Kompe, H. Borchert, J. Storz, A. Lobo, S. Adam, T. Moller, and M. Haase, *Angew. Chem. Int. Ed.* 42, 5513 (**2003**).
33. K. Riwotzki, H. Meyssamy, H. Schnablegger, A. Kornowski, and M. Haase, *Angew. Chem. Int. Ed.* 40, 573 (**2001**).
34. O. Lehmann, K. Kompe, and M. Haase, *J. Am. Chem. Soc.* 126, 14935 (**2004**).
35. X. Bai, H. W. Song, G. H. Pan, Z. X. Liu, S. Z. Lu, W. H. Di, X. G. Ren, Y. Q. Lei, Q. L. Dai, and L. B. Fan, *Appl. Phys. Lett.* 88 (**2006**).
36. Z. L. Wang, Z. W. Quan, P. Y. Jia, C. K. Lin, Y. Luo, Y. Chen, J. Fang, W. Zhou, C. J. O'Connor, and J. Lin, *Chem. Mater.* 18, 2030 (**2006**).
37. D. Y. Kong, Z. L. Wang, C. K. Lin, Z. W. Quan, Y. Y. Li, C. X. Li, and J. Lin, *Nanotechnology* 18 (**2007**).
38. M. M. Lezhnina, T. Justel, H. Katker, D. U. Wiechert, and U. H. Kynast, *Adv. Funct. Mater.* 16, 935 (**2006**).
39. A. Gedanken, R. Reisfeld, E. Sominski, O. Palchik, Y. Koltypin, G. Panczer, M. Gaft, and H. Minti, *J. Phys. Chem. B* 104, 7057 (**2000**).
40. A. Gedanken, R. Reisfeld, L. Sominski, Z. Zhong, Y. Koltypin, G. Panczer, M. Gaft, and H. Minti, *Appl. Phys. Lett.* 77, 945 (**2000**).
41. A. Patra, E. Sominska, S. Ramesh, Y. Koltypin, Z. Zhong, H. Minti, R. Reisfeld, and A. Gedanken, *J. Phys. Chem. B* 103, 3361 (**1999**).
42. V. G. Pol, R. Reisfeld, and A. Gedanken, *Chem. Mater.* 14, 3920 (**2002**).
43. X. Y. Chen, L. Yang, R. E. Cook, S. Skanthakumar, D. Shi, and G. K. Liu, *Nanotechnology* 14, 670 (**2003**).
44. X. Y. Chen, S. Skanthakumar, G. K. Liu, L. Yang, D. Shi, J. Lian, L. M. Wang, and R. E. Cook, Nanotechnology Focus, edited by E. V. Dirote, Nova Science Publishers, New York (**2005**), p. 141.
45. D. L. Shi, J. Lian, W. Wang, G. K. Liu, P. He, Z. Y. Dong, L. M. Wang, and R. C. Ewing, *Adv. Mater.* 18, 189 (**2006**).
46. J. Lian, L. Yang, X. Y. Chen, G. K. Liu, L. M. Wang, R. C. Ewing, and D. L. Shi, *Nanotechnology* 17, 1351 (**2006**).
47. P. Y. Jia, X. M. Liu, M. Yu, Y. Luo, J. Fang, and J. Lin, *Chem. Phys. Lett.* 424, 358 (**2006**).
48. M. Yu, H. Wang, C. K. Lin, G. Z. Li, and J. Lin, *Nanotechnology* 17, 3245 (**2006**).
49. G. Z. Li, M. Yu, Z. L. Wang, J. Lin, R. S. Wang, and J. Fang, *J. Nanosci. Nanotechnol.* 6, 1416 (**2006**).
50. P. Y. Jia, X. M. Liu, G. Z. Li, M. Yu, J. Fang, and J. Lin, *Nanotechnology* 17, 734 (**2006**).
51. H. Wang, C. K. Lin, X. M. Liu, J. Lin, and M. Yu, *Appl. Phys. Lett.* 87 (**2005**).
52. M. Yu, J. Lin, and J. Fang, *Chem. Mater.* 17, 1783 (**2005**).
53. C. K. Lin, B. Zhao, Z. L. Wang, M. Yu, H. Wang, D. Y. Kong, and J. Lin, *J. Nanosci. Nanotechnol.* 7, 542 (**2007**).
54. M. Nichkova, D. Dosev, S. J. Gee, B. D. Hammock, and I. M. Kennedy, *Anal. Chem.* 77, 6864 (**2005**).
55. M. Nichkova, D. Dosev, R. Perron, S. J. Gee, B. D. Hammock, and I. M. Kennedy, *Anal. Bioanal. Chem.* 384, 631 (**2006**).
56. N. C. Chang, *J. Appl. Phys.* 34, 3500 (**1963**).
57. N. C. Chang and J. B. Gruber, *J. Chem. Phy.* 41, 3227 (**1964**).
58. M. Buijs, A. Meyerink, and G. Blasse, *J. Lumin.* 37, 9 (**1987**).
59. J. Dexpert-Ghys, R. Mauricot, and M. D. Faucher, *J. Lumin.* 69, 203 (**1996**).
60. H. Y. Wang, R. J. Wang, X. M. Sun, R. X. Yan, and Y. D. Li, *Mater. Res. Bull.* 40, 911 (**2005**).
61. G. X. Liu and G. Y. Hong, *J. Solid State Chem.* 178, 1647 (2005).

62. X. Wang and Y. D. Li, *Angew. Chem. Int. Edit* 42, 3497 (**2003**).
63. L. Q. Liu, E. Ma, R. F. Li, G. K. Liu, and X. Y. Chen, *Nanotechnology* 18, 015403 (**2007**).
64. X. Y. Chen, H. Z. Zhuang, G. K. Liu, S. Li, and R. S. Niedbala, *J. Appl. Phys.* 94, 5559 (**2003**).
65. R. S. Meltzer and K. S. Hong, *Phys. Rev. B* 61, 3396 (**2000**).
66. X. Bai, H. W. Song, L. X. Yu, L. M. Yang, Z. X. Liu, G. H. Pan, S. Z. Lu, X. G. Ren, Y. Q. Lei, and L. B. Fan, *J. Phys. Chem. B* 109, 15236 (**2005**).
67. L. X. Yu, H. W. Song, S. Z. Lu, Z. X. Liu, and L. M. Yang, *Chem. Phys. Lett.* 399, 384 (**2004**).
68. X. Wang, X. M. Sun, D. P. Yu, B. S. Zou, and Y. D. Li, *Adv. Mater.* 15, 1442 (**2003**).
69. H. X. Mai, Y. W. Zhang, R. Si, Z. G. Yan, L. D. Sun, L. P. You, and C. H. Yan, *J. Am. Chem. Soc.* 128, 6426 (**2006**).
70. R. Si, Y. W. Zhang, L. P. You, and C. H. Yan, *Angew. Chem. Int. Ed.* 44, 3256 (**2005**).
71. R. Si, Y. W. Zhang, H. P. Zhou, L. D. Sun, and C. H. Yan, *Chem. Mater.* 19, 18 (**2007**).
72. L. Y. Wang and Y. D. Li, *Chem. Mater.* 19, 727 (**2007**).
73. H. Z. Wang, M. Uehara, H. Nakamura, M. Miyazaki, and H. Maeda, *Adv. Mater.* 17, 2506 (**2005**).
74. X. C. Jiang, L. D. Sun, and C. H. Yan, *J. Phys. Chem. B* 108, 3387 (**2004**).
75. X. Wang, J. Zhuang, Q. Peng, and Y. D. Li, *Nature* 437, 121 (**2005**).

Received: 15 November 2006. Accepted: 27 March 2007.